JOURNAL OF THERMOPHYSICS AND HEAT TRANSFER
Vol. 13, No. 1, January–March 1999

Sodium Vapor Pressure Losses in a Multitube, Alkali-Metal Thermal-to-Electric Converter

Jean-Michel Tournier* and Mohamed S. El-Genk†
University of New Mexico, Albuquerque, New Mexico 87131

A model was developed to calculate the vapor pressure losses and characterize the vapor flow regimes on the cathode side of a multitube, vapor–anode, alkali-metal thermal-to-electric converter (AMTEC) cell, with internal chevron's radiation shields. The dusty gas model was used to predict the vapor flow over a wide range of pressures, including the free-molecular, transition, and continuum flow regimes. Results showed that the vapor flow on the cathode side of a multitube AMTEC cell is typically in the transition regime, and that the pressure loss in the chevron's shield accounts for about 50% of the total pressure losses. An analysis is also performed to optimize the conical chevron's geometry for minimum pressure loss.

Nomenclature

A = surface area, m^2
a_{cc} = accommodation coefficient, Eqs. (1) and (25), 1
b = perpendicular distance between chevrons, m
D = flow diffusion coefficient, m^2/s
D_a = diameter of centerline liquid-return artery, m, 3.18 mm
D_B = BASE tubes outer diameter, m, 6.35 mm
D_e = equivalent hydraulic diameter, m
D_w = inner diameter of AMTEC cell wall, m, 33.2 mm
d = separation distance between chevrons, m
F = Faraday's constant, 96,485 C/mol
f = laminar friction coefficient
G = dimensionless geometric factor for pressure loss, Eq. (5)
I = total cell electrical current, A
J_r = electrode current density, A/m^2
Kn = Knudsen number of sodium vapor
L = effective flow path through chevrons, m
L_B = distance between bottom of electrode and top of BASE tube, m
L_C = distance between BASE tubes top and chevrons, m
L_S = height of chevron's shield, m
L_T = distance between chevrons and condenser, m
M = molecular weight of sodium, kg/mol, 23 gm/mol
Ma = vapor Mach number, $\dot{m}''_z/\sqrt{\gamma\rho P}$
$\dot{m}''_{\text{pore}}$ = vapor mass flux in electrode pores, kg/m^2 s
$\dot{m}_z$ = vapor axial mass flow rate, kg/s
$\dot{m}''_z$ = vapor axial mass flux, kg/m^2 s
N = number of conical chevrons
N_B = number of (seried-connected) BASE tubes, 7
P = sodium vapor pressure, Pa
Re = vapor Reynolds number, $D_e\dot{m}''_z/\mu$
R_g = perfect gas constant, 8.314 J/mol K
R_p = average hydraulic radius of electrode pores, m, 10 μm
T = temperature, K
t_E = thickness of cathode electrode, m, 5 μm
z = axial coordinate, m
α = chevrons packing factor, Fig. 3
$\bar{\alpha}_2$ = coefficient for advection of axial momentum
γ = specific heat ratio of sodium vapor, 5/3
ΔP = pressure loss through conical chevron's shield, Pa
ΔP_{cd} = pressure loss due to condensation of sodium, Pa
ΔP_E = pressure loss through cathode electrode, Pa
ΔP_{evap} = pressure loss as a result of evaporation of sodium at BASE surface, Pa
ε_E = volume porosity of cathode electrode, 0.9
ζ = correction factor for laminar flow in annulus
θ = angle of conical chevrons, Fig. 3
μ = dynamic viscosity of sodium vapor, kg/m s
ξ = resistance coefficient for sudden expansion, Eqs. (13) and (14)
ρ = vapor density (kg/m^3), $PM/(R_gT)$
φ = compressible factor, Eq. (26)
χ = flow conductance of chevron's shield, m^2/s

Subscripts
B = beta''-alumina solid electrolyte (BASE)
c = cathode electrode/BASE interface
cd = condenser
ev = evaporator
E = cathode electrode
z = axial direction
1 = BASE tubes/evaporator standoff bundle
2 = annular space above BASE tubes

Superscripts
in = inner surface, Eq. (19)
K = Knudsen flow regime
O = outer surface, Eq. (19)
vis = viscous (continuum) flow regime

Received Nov. 26, 1997; revision received May 22, 1998; accepted for publication May 22, 1998.

*Research Assistant Professor, Institute for Space and Nuclear Power Studies, Department of Chemical and Nuclear Engineering. Member AIAA.

†Regents' Professor, Department of Chemical and Nuclear Engineering, and Director, Institute for Space and Nuclear Power Studies. Senior Member AIAA.

Introduction

ALKALI-METAL thermal-to-electric converters (AMTEC) are being considered for future planetary exploration missions because of their potential for delivering electrical power at high conversion efficiency, in excess of 20–25%. The electrical power output of an AMTEC cell, which equals the work of isothermal expansion of sodium vapor through the β''-alumina solid electrolyte (BASE), is a logarithmic function of the ratio of the sodium vapor pressure on the anode (high-pressure) side to that on the cathode (low-pressure) side of the

BASE.[1] At typical condenser temperatures <650 K, the sodium vapor pressure on the cathode side is orders of magnitude lower (<50 Pa) than on the anode side (15–60 kPa, depending on the evaporator temperature, 950–1100 K). The sodium pressure at the interface between the BASE and cathode electrode is equal to the saturation pressure at the condenser plus the pressure losses caused by sodium vapor flow from the BASE surface to the condenser.

To increase the electric power output per cell, vapor–anode, multitube AMTEC cells are being tested at the U.S. Air Force Research Laboratory (AFRL), for meeting the electric power requirements of the NASA Pluto/Express (PX) spacecraft (to be launched in the year 2004) and future U.S. Air Force missions.[1] These cells typically have 5–7 BASE tubes each, and each BASE tube has anode and cathode metal TiN electrodes sputtered on the inside and outside surfaces, respectively (Fig. 1). The BASE tubes and the evaporator assembly are brazed to a stainless-steel support plate, and form a physical barrier between the high- and low-pressure zones. The porous electrodes are covered with copper or molybdenum mesh current collectors, to minimize internal electrical losses (Fig. 1b). Conduction and radiation from the support plate transport heat to the BASE tubes and evaporator structure. The chevron's radiation shield, placed above the tubes, reduces parasitic heat losses to the cell wall and condenser. A capillary wick structure recirculates the liquid sodium working fluid from the cell condenser to the evaporator (Fig. 1a).

An important input to the modeling of multitube, vapor–anode AMTECs is determining the pressure drop on the cathode side of the cell. As indicated earlier, the electric power output of the cell is a logarithmic function of the ratio of the anode vapor pressure to the cathode pressure. Therefore, the lower the pressure losses on the cathode side, the higher the cell's electrical power output.

Only a few investigators have attempted to calculate the vapor pressure losses on the cathode side of such AMTEC cells, owing to the complexity of the cell geometry (Fig. 1) and the fact that the vapor flow could be in the transition or the free-molecular regime.[2] Johnson[3] solved the Boltzmann conservation equation using a Monte Carlo method to calculate the vapor pressure losses in a single-tube AMTEC cell, with a remotely located condenser, internal heat shields, and a coaxial liquid return artery. Results showed that the vapor pressure drop on the cathode side of the cell varied proportionally with the sodium vapor mass flow rate, which is indicative of the free-molecular flow regime.

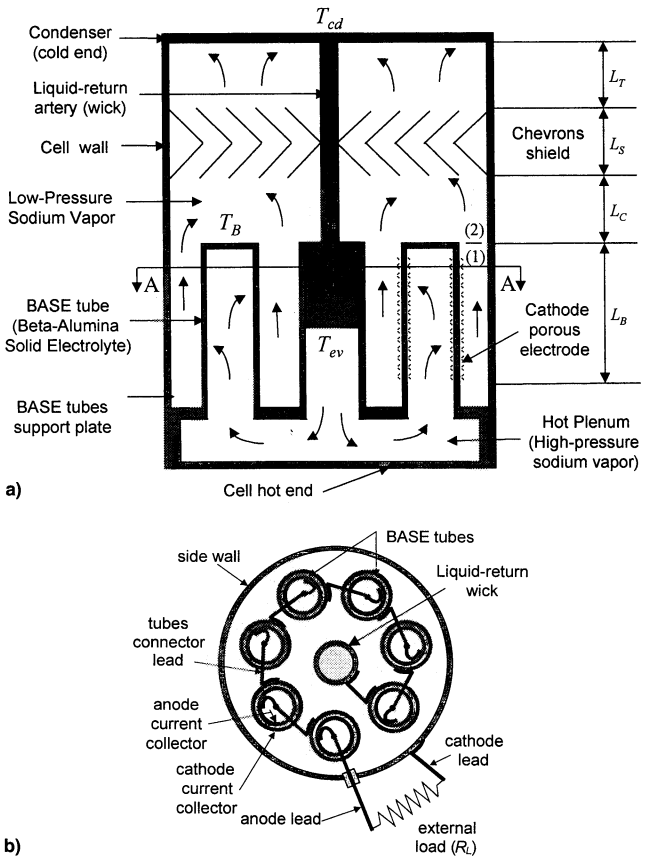

Fig. 1 Schematic of a multitube, vapor-anode AMTEC cell (not to scale): a) elevation and b) plan view (section A-A).

Ivanenok et al.[4] developed a vapor pressure loss model for a single-tube AMTEC, with an internal heat shield (disk) and a remote coaxial condenser tube. They assumed a continuum vapor flow having a parabolic radial velocity profile and corrected the laminar friction coefficient for a slip flow condition. The effect of increasing vapor mass flow rate along the BASE tube, because of the vapor perspiration at the BASE/cathode interface, was neglected. Their results compared reasonably well with measurements when the vapor flow upstream of the condenser was continuum or near continuum, which is the validity limit of the slip flow approximation. In current cell designs, however, where the vapor flow is expected to be in the transition or free-molecular regime, this approach is invalid, and can erroneously underpredict the vapor pressure losses.[2]

In an attempt to model the entire multitube, vapor–anode AMTEC cell, Schock et al.[5,6] developed complex thermal, electrical, and vapor flow models, using the SINDA thermal analyzer software and the ITAS radiation interchange code to calculate all radiation view factors in the cell. The vapor pressure losses, however, were calculated using a simplified approach based on the equivalent hydraulic diameter approximation and a general equation for all flow regimes. The calculated vapor pressure along the BASE tubes bundle dropped very quickly, from 43 to 14 Pa, causing the electrode current density along the BASE tubes to vary by a factor of 4. These results were in disagreement with the findings of the present authors, that the current density along the BASE tubes in a multitube AMTEC cell is closer to uniform.[1,7] Therefore, there is a need to develop a more appropriate vapor flow and pressure loss model for these cells.

In this paper, such a vapor flow model is developed based on the dusty gas model (DGM),[2] which has been verified for all vapor flow regimes of interest, continuum, transition, and molecular flow. The cell geometry used herein, the same as that used by Schock et al.,[6] has a hot plenum cavity that feeds seven BASE tubes with high-pressure sodium vapor, a remotely located condenser, and a centerline liquid-return artery (Fig. 1). The cell has also an internal chevron's radiation shield to reduce parasitic heat losses. In the present model, the flow diffusion coefficients in the free-molecular regime are calculated using the Dushman formulas, whereas those in the continuum regime are determined using an exact analytical solution (when available) or the equivalent hydraulic diameter approximation. The DGM is used to calculate the flow diffusion coefficients in the transition regime.

The present vapor flow model is used to calculate the pressure losses on the cathode side of the cell and to assess the effect of using a conical chevron's shield above the BASE tubes on the vapor pressure losses. For simplicity, the present analysis assumes uniform electrode current density and BASE temperature distributions. In a real cell, however, the electrode current density is slightly nonuniform and the temperature gradient along the BASE tubes is typically ~2 K/mm. The present vapor flow model has been successfully integrated into a full multitube AMTEC cell model, in which the predicted distributions of electrode current density and temperature along the BASE tubes are incorporated. The results of the integrated cell model (APEAM) have been benchmarked successfully with experimental data of several PX-series cells that have been tested in vacuum at AFRL.[1,7] APEAM's predictions of

the cells' electric power output were within ±10% of the measured values, at various hot- and cold-side temperatures.

Sodium Vapor Flow Model Description

The vapor pressure drop between the BASE/cathode interface and the remote condenser is calculated as the sum of the following contributions (Fig. 1):

1) The evaporation of sodium at the BASE outer surface, $\Delta P_{evap}(z)$.
2) Vapor perspiration through the porous cathode electrode, $\Delta P_E(z)$.
3) Vapor flow along the BASE tubes/evaporator standoff bundle, $[P_1(0) - P_1(L_B)]$.
4) Sudden change in the cross-sectional flow area at the top of BASE tubes, $[P_1(L_B) - P_2(L_B)]$.
5) Vapor flow in the annulus above the BASE tubes, below the conical chevron's shield, $[P_2(L_B) - P_2(L_B + L_C)]$.
6) Vapor flow through the conical chevron's radiation shield, $\Delta P = [P_2(L_B + L_C) - P_2(L_B + L_C + L_S)]$.
7) Vapor flow in the annulus between the top of the chevron's shield and the cell condenser.
8) Condensation of sodium vapor at the cold end of the cell, ΔP_{cd}.

Pressure Drop Caused by Evaporation of Sodium at BASE Surface

The pressure drop caused by the evaporation of sodium along the BASE/cathode interface was given by the kinetic theory of gases[2]

$$P_1(z) - P_2(z) = a_{cc}\left(\frac{2\pi R_g T}{M}\right)^{1/2} \dot{m}''_{pore}(z)$$

where

$$\dot{m}''_{pore}(z) = \frac{M}{\varepsilon_E F} J_r(z) \tag{1}$$

The accommodation coefficient, a_{cc}, for liquid metals is close to unity in well-evacuated, clean systems (such as in heat pipes[2] or AMTEC).

Pressure Drop in the Porous Electrode (Cathode)

The pressure drop caused by vapor flow through the porous electrode (cathode) was calculated using the DGM[2]:

$$\Delta P_E(z) = \frac{t_E}{D}\left(\frac{R_g T}{M}\right) \times \dot{m}''_{pore}(z) \tag{2}$$

The flow diffusion coefficient, D, is given by

$$D = D^{vis} + D^K \times \frac{1 + c_1^K \bar{P}}{1 + c_2^K \bar{P}} \tag{3}$$

In Eq. (3), $\bar{P}$ is the average vapor pressure in the pores of the cathode electrode. The viscous and free-molecular flow diffusion coefficients are given, respectively, as[2,8]

$$D^{vis} = a^K \bar{P} = \frac{R_p^2}{8\mu}\bar{P}$$

$$D^K = \frac{20 + 8(t_E/R_p)}{20 + 19(t_E/R_p) + 3(t_E/R_p)^2} \times \frac{t_E}{4} \times \left(\frac{8R_g T}{\pi M}\right)^{1/2} \tag{4a}$$

where

$$c_2^K = \frac{4R_p}{\mu} \times \left(\frac{M}{R_g T}\right)^{1/2}, \qquad c_1^K = 0.81 \times c_2^K \tag{4b}$$

The DGM has been shown to accurately predict the pressure drop for gas flow in capillary tubes, in all three flow regimes.[2] At very low vapor pressure D reduces to the Knudsen diffusion coefficient for free-molecular flow, which is independent of pressure. At high pressure ($Kn < 0.02$), however, the Knudsen diffusivity is small compared with the viscous flow diffusivity, which increases proportionally with the vapor pressure, and the flow becomes essentially continuum.

Some metal electrodes do not have an apparent porosity, and the sodium atoms are transpired to the surface of the electrode by molecular diffusion. In such cases, the pressure drop in the electrode is expressed in terms of an empirical geometrical factor, G_E, as

$$\Delta P_E(z) = \frac{3G_E}{8\pi}\left(\frac{2\pi R_g T}{M}\right)^{1/2} \times \frac{M}{F} J_r(z) \tag{5}$$

The factor G_E is determined experimentally, and varies typically between 10 and 60.

Pressure Drop Along the BASE Tubes

The vapor space between the BASE tubes and the evaporator standoff in the AMTEC cell (Fig. 1) is treated as a single channel having an equivalent hydraulic diameter,[9] D_e. The increase in vapor mass flow rate per unit length of the BASE tubes is given by

$$\frac{d\dot{m}_z(z)}{dz} = (N_B \pi D_B) \times \frac{M}{F} J_r(z) \tag{6}$$

The conservation of axial momentum is expressed as[2]

$$\bar{\alpha}_2 \frac{d}{dz}\left(\frac{\dot{m}''^2_z}{\rho}\right) = -\frac{dP_1}{dz} - \left(\frac{R_g T}{M}\right)\frac{\dot{m}''_z}{D} \tag{7}$$

The coefficient $\bar{\alpha}_2$ in Eq. (7) accounts for the nonuniform axial velocity profile of vapor, and is a function of Kn.[2] A value $\bar{\alpha}_2 = 1$ was used in the present work because the advection of axial momentum represented less than 8% of the total calculated pressure loss. D was given by the first approximation of the DGM, for which $c_1^K = c_2^K = 0$, thus, $D = D^{vis} + D^K$. For flow in circular channels, the first approximation results in a maximum error of less than 10% in the transition flow region, when compared with experimental data.[2] The viscous flow diffusion coefficient, D^{vis}, was expressed in terms of the friction coefficient, f, as

$$D^{vis} = \frac{2D_e}{\dot{m}''_z f} P_1 \tag{8}$$

The vapor pressure above the BASE tubes is typically less than 20 Pa, and Mach number >0.2 can be encountered, thus the vapor flow is compressible. The viscous friction coefficient was corrected for the effect of compressibility using the von Kármán correction[9]

$$f = \frac{64\mu}{D_e \dot{m}''_z}\left(1 + \frac{\gamma - 1}{2} Ma^2\right)^{-1/2} \tag{9}$$

Approximate formulas for molecular flows through channels and apertures of any shapes were developed principally by Knudsen using the kinetic theory of gases. The diffusion coefficient for free-molecular flow through a channel of length, L, and cross section, A,[8] is

$$D^K = \frac{L}{1 + (3L/4D_e)}\left(\frac{R_g T}{2\pi M}\right)^{1/2} \tag{10}$$

Table 1 Resistance coefficient ξ for sudden expansions of different area ratios[10]

Area ratio, $\beta = A_1/A_2$	$Re_1 = 1$		$Re_1 = 5$		$Re_1 = 10$		ξ selection
	K, exp	ξ,[a] exp	K, exp	ξ,[a] exp	K, exp	ξ,[a] exp	
0.05	3714	3714	740	3700	340	3400	3700
0.16	512	512	110	550	51	510	512
0.43	127	127	27.4	137	11.9	119	127
0.64	66.3	66.3	15.0	75.0	7.05	70.5	69

[a] $\xi = K \times Re_1$.

Although Eq. (10) is only approximate, it agrees well with experimental data and Monte Carlo calculation results for flow channels of various cross sections and shape.[8] The use of Eq. (10) (the Dushman formula) for circular tubes results in a maximum error of 11.4% at a length to diameter ratio, $L/D_e = 2$. For 90-deg bent elbows, annuli, rectangular louvers, and chevrons' baffles, the error is less than 10%.[8] The compressible term on the left-hand side of Eq. (7) could be written

$$\frac{d}{dz}\left(\frac{\dot{m}_z''^2}{\rho}\right) = \frac{\dot{m}_z''^2}{\rho}\left(\frac{1}{T}\frac{dT}{dz} - \frac{1}{P_1}\frac{dP_1}{dz} + \frac{2}{\dot{m}_z''}\frac{d\dot{m}_z''}{dz}\right) \tag{11}$$

Combining Eqs. (7) and (11) gave the following expression for the sodium pressure gradient:

$$\frac{dP_1}{dz} = -\frac{1 + \bar{\alpha}_2 \dfrac{\dot{m}_z'' D}{P_1}\left(\dfrac{1}{T}\dfrac{dT}{dz} + \dfrac{2}{\dot{m}_z''}\dfrac{d\dot{m}_z''}{dz}\right)}{1 - \bar{\alpha}_2\left(\dfrac{R_g T}{M}\right)\left(\dfrac{\dot{m}_z''}{P_1}\right)^2}\left(\frac{R_g T}{M}\right)\frac{\dot{m}_z''}{D} = \Phi(P_1, z) \tag{12}$$

Equation (12) expresses the vapor pressure gradient in terms of the local vapor pressure, $P_1(z)$. Because the current density and BASE temperature distributions are known, the local sodium vapor mass flow rate can be calculated by integrating Eq. (6). Therefore, all terms on the right-hand-side (RHS) of Eq. (12) are known, except the local vapor pressure. Equation (12) was integrated numerically using the trapezoidal rule to obtain the axial distribution of the vapor pressure along the BASE tubes. The total length of the BASE tubes was discretized into n identical sections. Results showed that the pressure drop obtained with $n = 20$ was within <1% of the value calculated with an arbitrarily large number of elements ($n = 500$).

Pressure Loss Caused by Sudden Expansion at Top of BASE Tubes

At typical operating conditions in AMTEC cells, the vapor Reynolds number is less than 1.3×10^1, and the pressure drop caused by the sudden expansion at the top of BASE tubes was calculated as[10]

$$P_1(L_B) - P_2(L_B) = K\tfrac{1}{2}(\dot{m}_z''^2/\rho)_1$$

where

$$K = \xi(\mu/D_e \dot{m}_z''^{\max})_1 \tag{13}$$

Measured values of the resistance coefficient, ξ, are listed in Table 1 for an expansion area ratio of 0.05, 0.16, 0.43, and 0.64. The selected values of ξ were used to obtain the following empirical relation:

$$\xi = 1908 \times (\beta - 0.145)^{-0.05812} - 1923 \tag{14}$$

As shown in Fig. 2, Eq. (14) fits the exponential dependence of the resistance coefficient on the expansion area ratio, β.

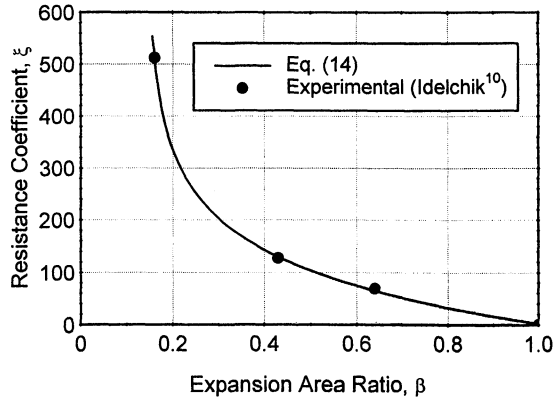

Fig. 2 Resistance coefficient ξ for sudden expansion as a function of area ratio.

Pressure Loss in Annulus Above BASE Tubes

The vapor flow rate in the annulus above the BASE tubes is constant and equal to that at the top of BASE tubes. In this annulus, the conservation of axial momentum can also be expressed by Eq. (7). D in this region was obtained from the first approximation of the DGM as

$$D = D^{\text{vis}} + D^K = \frac{D_e^2}{32\mu}\sqrt{1 + \frac{\gamma - 1}{2}Ma^2} \times \frac{P_2}{\zeta} + \frac{L_C}{1 + (3L_C/4D_e)}\left(\frac{R_g T}{2\pi M}\right)^{1/2} \tag{15}$$

For viscous laminar flow in annular channel, the correction factor, ζ, has the expression[9]

$$\zeta = (D_w - D_a)^2\left[D_w^2 + D_a^2 - \frac{D_w^2 - D_a^2}{\ell n(D_w/D_a)}\right]^{-1} \tag{16}$$

This factor varies between 1.0 and 1.5, which indicates that, for laminar flow, the calculated vapor pressure loss based on the equivalent diameter approximation could be in error by as much as 33%, if ζ is not included, i.e., $\zeta = 1$. The diffusion coefficient for free-molecular flow, D^K, was calculated using the Dushman formula [Eq. (10)]. For annular flow, this equation is within 10% of numerical results obtained by the Monte Carlo method.[8]

Finally, the pressure gradient in the annulus preceding the BASE tubes was expressed as

$$\frac{dP_2}{dz} = -\frac{1 + \bar{\alpha}_2 \dfrac{\dot{m}_z'' D}{P_2}\left(\dfrac{1}{T}\dfrac{dT}{dz}\right)}{1 - \bar{\alpha}_2\left(\dfrac{R_g T}{M}\right)\left(\dfrac{\dot{m}_z''}{P_2}\right)^2}\left(\frac{R_g T}{M}\right)\frac{\dot{m}_z''}{D} = \Phi(P_2, z) \tag{17}$$

Equation (17) expresses the vapor pressure gradient in the annulus in terms of the local vapor pressure, $P_2(z)$. All other terms on the RHS of Eq. (17), which involve the sodium mass flow rate and temperature distribution, are known. Equation

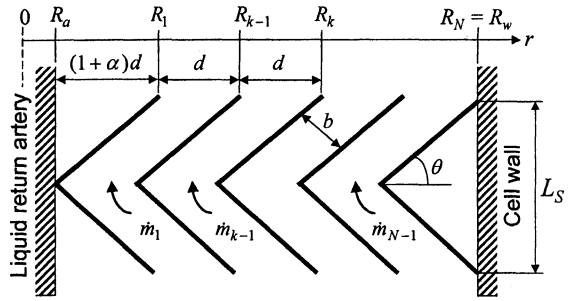

Fig. 3 Schematic of (unseparated) conical chevron's radiation shield.

(17) was integrated numerically to obtain the axial distribution of the sodium vapor pressure, $P_2(z)$, in the annulus above the BASE tubes. Numerical results showed that the pressure distribution obtained with $n = 20$ was within <1% of that calculated with an arbitrarily large number of elements ($n = 500$).

Pressure Loss Caused by Vapor Flow Through Chevron's Shield

Midway between the BASE tubes and condenser, N conical chevrons that are $(1 + \alpha)d$ wide and separated by a distance d, were placed to reduce parasitic radiation losses from the BASE tubes to the cell wall and to the condenser (Fig. 1). The conical chevrons were arranged such that $(N + \alpha) = (R_w - R_a)/d$, and there were $(N - 1)$ conical flow passages (Fig. 3). The conservation of vapor flow through the chevrons was expressed as

$$\dot{m}_z = \sum_{k=1}^{N-1} \bar{A}_k \dot{m}_k'' \tag{18}$$

The perpendicular distance between chevrons is $b = d \sin(\theta)$, and the effective path length of every passage is $L = (1 + \alpha)2d/\cos(\theta)$. From a hydrodynamic point of view, every conical flow passage (k) is equivalent to an effective annulus having a flow area $\bar{A}_k$; average perimeter $\bar{S}_k$; equivalent hydraulic diameter D_{ek}; and inner and outer diameters, respectively, D_k^{in} and D_k^{out}. The effective flow area of an inclined annulus having an inner radius R is $A(R) = \pi b(2R + b \sin \theta)$. Introducing $R_k = R_a + d \times (k + \alpha)$, as the radius of the chevron (k) at the entrance of the shield, the average flow area of the passage (k) can be calculated by averaging $A(R)$ between $R_k - (1 + \alpha)d$ and R_k, as $\bar{A}_k = \pi b[2R_k - d(\alpha + \cos^2\theta)]$. The perimeter of an equivalent chevron annulus with an inner radius R is $S(R) = 2\pi(2R + b \sin \theta)$, and the average perimeter was calculated as $\bar{S}_k = 2\pi[2R_k - d(\alpha + \cos^2\theta)]$. Then, $D_{ek} = 4\bar{A}_k/\bar{S}_k = 2b$. Finally, we obtained

$$\begin{aligned} D_k^{in} &= 2R_k - b - d(\alpha + \cos^2\theta) \\ D_k^{out} &= 2R_k + b - d(\alpha + \cos^2\theta) \end{aligned} \tag{19}$$

The conservation of axial momentum in the annular passage (k) of the chevrons was expressed as

$$\left[1 - \bar{\alpha}_2 \left(\frac{R_g T}{M}\right) \frac{\dot{m}_k''^2}{P_k^2}\right] \frac{dP_k}{dz} = -\left(\frac{R_g T}{M}\right) \frac{\dot{m}_k''}{D_k} \tag{20}$$

where the flow diffusion coefficient, D_k, was given by Eq. (15), as

$$D_k = D_k^{vis} + D_k^K = \frac{b^2}{8\mu} \sqrt{1 + \frac{\gamma - 1}{2} Ma_k^2} \times \frac{P_k}{\zeta_k} + \frac{L}{1 + (3L/8b)} \left(\frac{R_g T}{2\pi M}\right)^{1/2} \tag{21}$$

For the sodium flow rates typically encountered in PX-series AMTEC cells (Fig. 1), the solution can be greatly simplified. The compressible term in Eq. (20) can be neglected. Also, because the von Kármán compressible factor varies within a very narrow range, between 1.0 and 1.013, at typical vapor Mach numbers <0.28, it can also be neglected in Eq. (20); hence, the expression for D_k is simplified as

$$D_k = D_k^{vis} + D_k^K = a_k^K P_k + D^K \tag{22}$$

The coefficient a_k^K and the Knudsen diffusion coefficient, D^K, are independent of the sodium vapor pressure and mass flux. With these simplifications, the integration of Eq. (20) along a chevron's flow passage (k) having a flow path length, L, gives the vapor pressure loss term as

$$\Delta P_k = \left(\frac{R_g T}{M}\right) \frac{L}{\overline{D_k}} \dot{m}_k'' = \Delta P, \qquad \text{for} \quad k = 1 \quad \text{to} \quad (N - 1) \tag{23}$$

$\overline{D_k}$ was evaluated at the average vapor pressure in the chevrons, $\bar{P}_k = P_2(L_B + L_C) - \Delta P/2$. The pressure loss through the chevrons was obtained by substituting Eq. (23) into the sodium vapor mass balance, Eq. (18), and rearranging the results as

$$\Delta P = \frac{1}{\chi} \left(\frac{R_g T}{M}\right) \dot{m}_z$$

where

$$\chi = \sum_{k=1}^{N-1} A_k \overline{D_k}/L \tag{24}$$

Pressure Loss Caused by Condensation of Sodium

The pressure drop caused by the condensation of sodium vapor onto the condenser surface (Fig. 1) was obtained from the kinetic theory of gases[2]

$$\Delta P_{cd} = a_{cc} \left(\frac{2\pi R_g T_{cd}}{M}\right)^{1/2} \dot{m}_z'' \tag{25}$$

Results and Discussion

The present sodium vapor pressure loss model was used to characterize the flow regime and calculate the pressure losses on the cathode side of a multitube AMTEC cell (Fig. 1). Also, the effect of a conical chevron's shield above the BASE tubes on the vapor pressure losses was evaluated. The vapor temperature above the BASE tubes (on the cathode side) was assumed to vary linearly between the BASE and the condenser temperatures. The multitube, vapor-anode AMTEC cell that was analyzed had seven series-connected BASE tubes (o.d. = 6.35 mm), covered with 15.88 mm-high electrodes, having an effective $G_E = 11.7$ [Eqs. (2), (4a), and (5) with $t_E = 5$ μm, $R_p = 10$ μm, and $\varepsilon_E = 0.9$]. The o.d. of the evaporator standoff was equal to that of BASE tubes (Fig. 1). The diameters of the cell wall and liquid-return artery were 33.2 and 3.18 mm, respectively, and the condenser was placed 61 mm away from the top of the BASE tubes. A chevron's radiation shield, consisting of four conical chevrons with a 45-deg angle, was placed above the BASE tubes. In the minimum shielding configuration of direct radiation between BASE tubes and condenser, $\alpha = 0$, and $L_S = 7.5$ mm.

Vapor Pressure Losses in a Multitube, Vapor-Anode AMTEC Cell

Figure 4 shows the calculated sodium vapor pressure on the cathode side of the multitube AMTEC cell, at condenser and BASE tube temperatures of 550 and 1050 K, respectively, for three different placements of the chevrons, and without thermal shield. The cell electric current was fixed at $I = 1.39$ A,

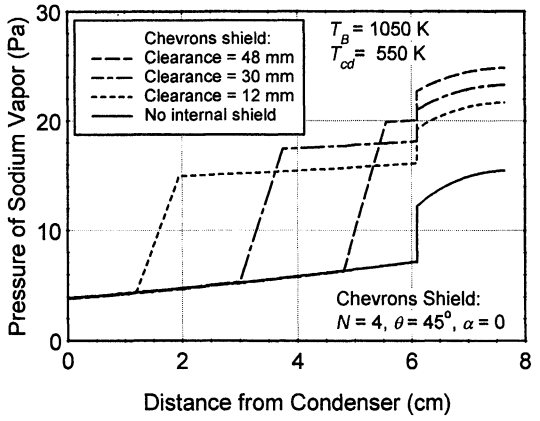

Fig. 4 Calculated vapor pressure on cathode side of a multitube AMTEC cell (I = 1.39 A, $\dot{m}_z$ = 8.3 g/h).

which corresponds to a sodium mass flow rate of 8.3 g/h. Calculated pressure losses for a shield clearance of 48 mm (the distance between condenser and top of radiation shield) are also listed in Table 2. As shown in Fig. 4, the axial pressure profile of sodium vapor along the BASE tubes was parabolic, owing to continuous mass addition at the BASE tubes outer surface. The major contributions to the pressure losses between the condenser and BASE surface were those due to chevron's shield (50.6%), condensation of sodium vapor (11.1%), and the sudden expansion at top of BASE tubes (9.7%).

The closer the shield was to the BASE tubes, the larger the total vapor pressure losses on the cathode side, because the vapor pressure loss through the chevrons increased with the vapor temperature in the shield. In the case with no internal shield, the sodium pressure at the BASE/cathode electrode interface was much lower (by about 8 Pa) than in the cases with shields (Fig. 4).

The calculated sodium vapor flow characteristics on the cathode side of the multitube AMTEC cell with chevrons shield are shown in Fig. 5 for T_{cd} = 550 K, T_B = 1050 K, I = 1.39 A, and a 30-mm shield clearance. The vapor temperature in the pores of the cathode electrode and in the bundle of BASE tubes/evaporator standoff was assumed equal to that of the BASE tubes. Above these tubes, the vapor temperature was assumed to vary linearly between T_B and T_{cd} (Fig. 5a). The sodium vapor flow regime in the AMTEC cell is characterized by the value of the Knudsen number, Kn, ratio of the molecules mean free path, λ, to the channel equivalent diameter D_e. A Knudsen number below 0.01 indicates a continuum flow regime, whereas the free-molecular regime typically occurs at $Kn > 1$.[2] As shown in Fig. 5b, the vapor flow in the multitube AMTEC cell was in the transition regime, with Kn ranging between 0.04 and 0.4. Kn is proportional to the vapor temperature, and inversely proportional to the vapor pressure and D_e. Kn decreased sharply above the BASE tubes because of the increase in D_e (Fig. 5b). It increased again as the vapor flowed through the chevron's shield. In the annular space above the BASE tubes, Kn decreased slowly because of the decrease in vapor temperature (the vapor pressure remained essentially constant because pressure losses were small in the annulus, Fig. 4). However, Kn was higher between the shield and the condenser because the vapor pressure was much smaller there than between the BASE tubes and the chevron's shield. Figure 5c shows the calculated flow diffusion coefficients along the cell. These coefficients are functions of vapor temperature and pressure, mass flow rate, and D_e. The total flow diffusion coefficient is the sum of the viscous and Knudsen flow coefficients. As Fig. 5c shows, the viscous and Knudsen flow diffusion coefficients were of the same magnitude in the channels of a small equivalent hydraulic diameter (BASE tubes bundle and chevron's shield), whereas the viscous flow diffusion coefficient was about one order of magnitude larger than the Knudsen flow diffusion coefficient in the wider annulus above the BASE tubes, where the flow was more viscous.

Table 2 Sodium vapor pressure losses in PX-1A cell[a]

Region/process	Pressure drop, Pa	Fraction, %
Condensation	3.0	11.1
Between condenser and chevrons	2.5	9.3
Through chevrons	13.6	50.6
Between chevrons and tubes	0.2	0.7
Expansion above BASE tubes	2.6	9.7
BASE tubes/standoff[b]	1.0	3.7
Through cathode electrode	2.2	8.2
Evaporation at BASE surface	1.8	6.7
Total pressure drop[b]	26.9	100

[a]With four (48-mm clearance) 45-deg-angle chevrons (condenser vapor pressure = 0.8 Pa, T_{cd} = 550 K, T_B = 1050 K, and I = 1.39 A).
[b]Between condenser and BASE surface (at midplane of electrode).

The sodium mass flow rate increased linearly along the cathode electrode, reaching its maximum value of 8.3 g/h at the top of the BASE tubes, which corresponded to I = 1.39 A (Fig. 5d). The electrode current density was assumed uniform, J_r = 0.439 A/cm^2. As shown in Fig. 5e, the axial Reynolds number of the vapor flow increased with the mass flow rate along the BASE tubes. Above the BASE tubes, Re was higher because of the smaller wetted perimeter of the annular can, but increased steadily toward the condenser, because of the decrease in the vapor temperature. The vapor Reynolds number was much lower in the chevron's shield, because of the change in geometry (the smaller channels of the shield have lower equivalent hydraulic diameter). The maximum Reynolds number, $Re = 1 \times 10^1$, occurred at the condenser. The flow of sodium vapor was laminar throughout the cell, and was slow enough to justify the use of Idelchik's relation [Eq. (13)] for evaluating the pressure drop resulting from the sudden expansion at the top of BASE tubes.

The vapor Mach number is proportional to the mass flow rate and the square root of temperature, and inversely proportional to the flow cross-sectional area and vapor pressure. As shown in Fig. 5f, the vapor Mach number reached its largest value of 0.25 at the condenser. At such a Mach number, the von Kármán correction factor for compressible effects varied between 1 and 1.01 and could be neglected. The following compressible factor φ appearing in the axial momentum conservation Eqs. (12), (17), and (20), was less than 1.3% in the bundle of BASE tubes/evaporator standoff, and less than 1.0% in the annulus between BASE tubes and chevrons shield:

$$\varphi = \bar{\alpha}_2 \left(\frac{R_g T}{M}\right)\left(\frac{\dot{m}''_z}{P}\right)^2 \tag{26}$$

The calculated value of φ in the chevrons' channels was only 7.0%, which justifies neglecting it in the development of the shield pressure drop model. The compressible factor reached its larger values in the annular space between the chevrons and the condenser, where the pressure was lowest. In this zone, φ varied between 7.0 and 10.0%.

For a radiation shield clearance of 48 mm, results showed that the multitube AMTEC cell has an effective geometric factor, G, for the total pressure losses on the cathode side:

$$G = \frac{\Delta P_{c,\text{loss}}}{\Delta P_E} \times G_E = \frac{26.9}{2.2} \times 11.7 = 143 \tag{27}$$

Results showed that the total pressure drop on the cathode side of the multitube AMTEC cell varied linearly with I, which is a characteristic of free-molecule and transition flow regimes. An examination of Eqs. (3), (4), (8), (10), (15), and (21–24) indicates that the flow diffusion coefficients are very weak functions of the vapor mass flow rate in these regimes. The

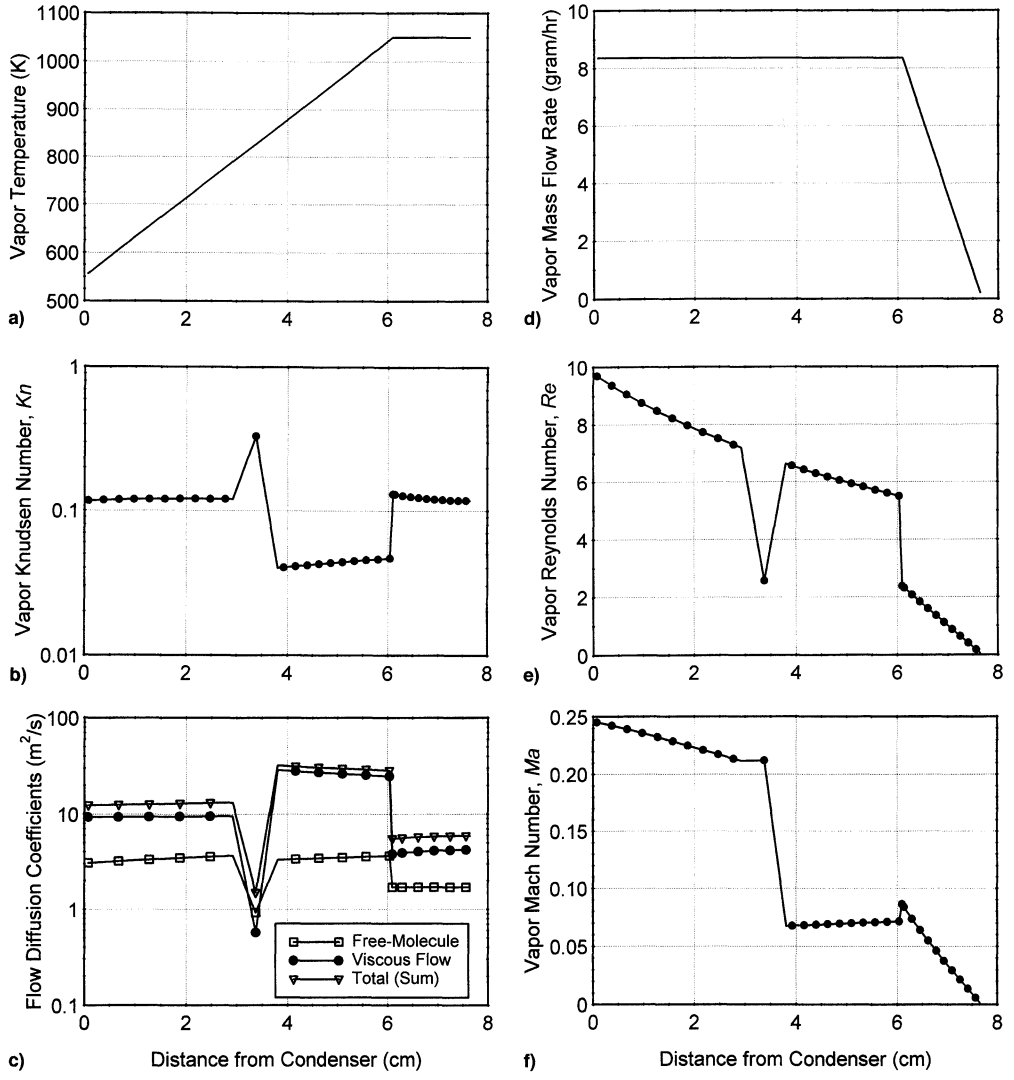

Fig. 5 Sodium vapor flow characteristics in a multitube vapor–anode AMTEC cell with a chevron's shield (T_{cd} = 550 K, T_B = 1050 K, 30-mm shield clearance, I = 1.39 A, $\dot{m}_z$ = 8.3 g/h): a) vapor temperature, b) *Kn*, c) flow diffusion coefficients, d) $\dot{m}_z$, e) *Re*, and f) *Ma*.

present findings are in agreement with that of Johnson,[3] who solved the Boltzmann equation using a Monte Carlo method to calculate the vapor pressure losses in a single-tube cell. The present results show that the total pressure drop on the cathode side of a multitube cell can be accurately predicted using Eq. (5).

Optimization of Conical Chevron's Shield in Multitube AMTEC Cell

The vapor pressure loss model described in the previous section was used to evaluate the effect of chevrons geometry on the sodium vapor pressure drop through the shield. Several configurations were investigated.

Conical Chevrons in Minimum Configuration (α = 0)

The first case investigated was that of the configuration that ensured minimum blockage of all direct radiation between BASE tubes and condenser, for which the distance between chevrons, d, is equal to the width of the conical chevrons, that is when α = 0 (Fig. 3). Figure 6 shows the required height of the chevrons as a function of number of chevrons, N, and angle of chevrons, θ. The larger the angle of chevrons, the taller the shield must be for the chevrons to cover the annular space for any direct radiation path. Similarly, the smaller the number of chevrons, the taller they must be (Fig. 3). The flow conductance of the chevron's shield, χ, is plotted in Fig. 6 as a function of θ and N, at typical temperature and pressure of 950 K

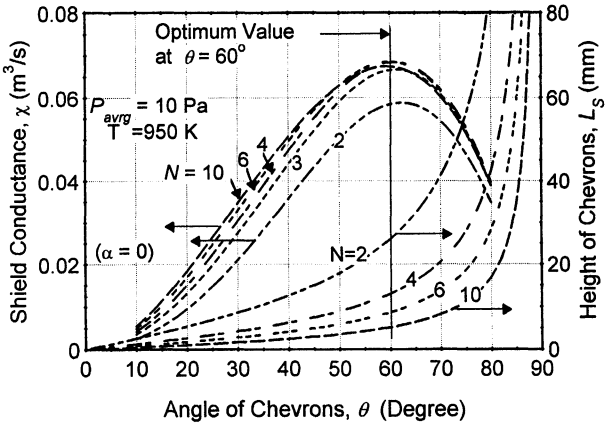

Fig. 6 Shield flow conductance χ and chevron's height as a function of angle θ and number of chevrons N (α = 0).

and 10 Pa, respectively. As this figure shows, the conductance χ peaked at a chevron angle of 60 deg. This maximum was virtually independent of the number of chevrons N, for values of N greater than 3. Figure 7 shows the resulting pressure drop in the chevron's shield at a typical cell current of 1.67 A (or a sodium mass flow rate of 10 g/h), as a function of θ and N. The minimum pressure drop of 14 Pa occurred at a chevron

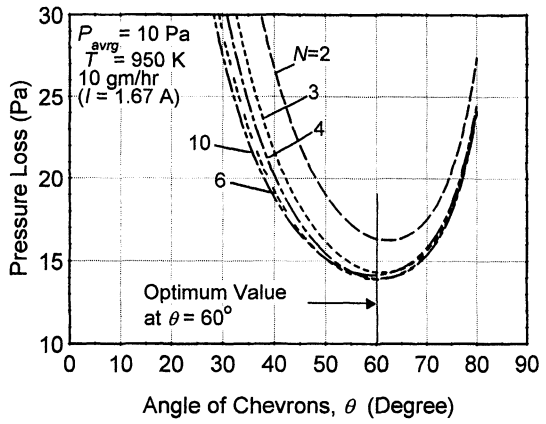

Fig. 7 Pressure loss through unseparated radiation shield as a function of angle θ and number of chevrons N (α = 0).

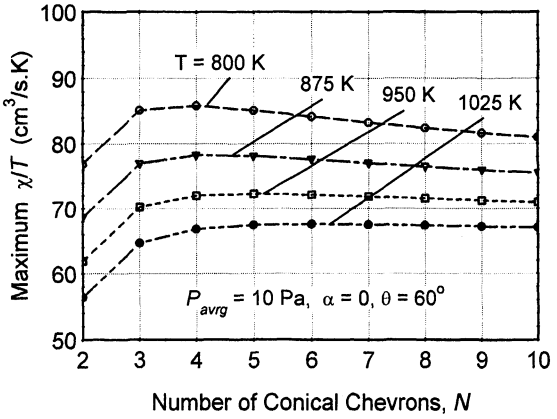

Fig. 8 Effects of temperature and number of chevrons on the pressure loss through radiation shield (α = 0, θ = 60 deg).

angle of 60 deg. This minimum pressure drop was not particularly sensitive to the angle near the optimum, allowing some tolerance in manufacturing. For example, using a shield with angle of 50 or 70 deg only resulted in an increase in pressure drop of 1 Pa, or 7% of the minimum pressure drop (Fig. 7). Also, the minimum pressure drop was independent of the number of chevrons N, for $N > 3$.

The effect of temperature on the flow conductance of the chevron's shield is illustrated by Fig. 8, for a shield with optimum 60-deg-angle chevrons. The pressure drop through the chevron's shield increased with temperature and, therefore, with the distance between the shield and the condenser. For example, a 75 K increase in chevron's temperature increases the pressure drop by 8%. Figure 8 also shows the effect of N on χ. It peaked at N = 4 or 5, then decreased slowly with increasing N.

Crowded Chevrons Configuration ($\alpha > 0$)

The case investigated previously was that of the configuration geometry that ensured minimum blockage of all direct radiation between the BASE tubes and condenser (α = 0). However, one would expect the radiative function of the shield to improve as the chevrons are packed closer to each other, $\alpha > 0$ (Fig. 3). The effects of the packing factor, α, and the number of chevrons, N, on the vapor pressure loss through the shield are shown in Fig. 9 for a 60-deg-angle chevron's shield. The pressure drop increased with increasing α. The larger the value of α, the larger the optimum number of N. As an illustration, consider first the optimum case of four 60-deg-angle chevrons with α = 0 (N = 4). The conical chevrons would be 13 mm in height, and the flow path L = 15 mm. Consider now a configuration of five 60-deg-angle chevrons of identical

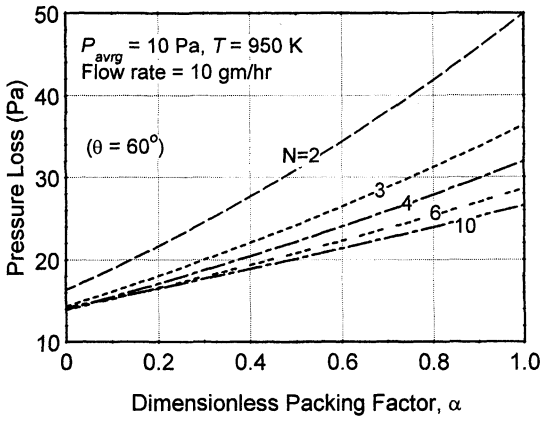

Fig. 9 Calculated pressure loss through radiation shield as a function of packing factor α and N (θ = 60 deg).

height, L_S = 13 mm (N = 5). To make room for the additional (fifth) chevron, it is necessary to move the chevrons closer to each other, with a packing factor of α = 1/3. The addition of a fifth chevron of identical height caused a 36% increase in the pressure drop, from 14 to 19 Pa (Fig. 9).

Pressure Losses Through Separated Conical Chevrons

Another shield geometry of interest is that of separated conical chevrons. In this geometry, the backward and forward halves of the chevrons are not welded together, but are separated some distance from each other. This configuration is equivalent to two chevron's shields of identical flow path ($L/2$) in series. Examination of Eq. (21) shows that the viscous flow diffusion coefficient remains unchanged, while the path length, L, appearing in the expression of the Knudsen flow diffusion coefficient, is replaced by $L/2$. The expression for the pressure drop [Eq. (24)] remains unchanged because L is replaced by $L/2$ in this equation, but the pressure drop must be multiplied by 2 to account for both sections of the shield. In the end, the only difference between separated and nonseparated chevron's geometries is the value of the path length in the expression of the Knudsen flow diffusion coefficient. Because the latter is an increasing function of path length, one expects separated chevrons to have a larger pressure drop than nonseparated chevrons. The calculated vapor pressure loss through separated conical chevrons, at a typical sodium mass flow rate of 10 g/h, a temperature and pressure of 950 K and 10 Pa, respectively, and a minimum configuration (α = 0), reached a minimum at an angle of 62 deg, for a separated shield with three or four chevrons. The minimum pressure drop, 17 Pa, was 22% larger (3 Pa above) than that for nonseparated chevrons.

Summary and Conclusions

A detailed model was developed for calculating the vapor pressure losses and characterizing the flow regimes on the cathode side of multitube vapor–anode AMTEC cells. The model used the DGM and predicted the vapor flow over a wide range of pressures, including the free-molecular, transition, and continuum flow regimes. Results showed that the vapor flow in a multitube AMTEC cell was in the transition regime, with Knudsen numbers ranging between 0.04 and 0.4. At a sodium mass flow rate of about 9 g/h, the Re was less than 1×10^1. The vapor axial Mach number peaked at 0.25 at the condenser, a value low enough to justify neglecting the vapor compressible effects in the conical chevron's shield model.

Results also showed that the pressure loss through the chevron's radiation shield dominated, by far, all other pressure losses, contributing more than half the total pressure losses between the condenser and cathode/solid electrolyte surface. The total vapor pressure drop in the cell varied linearly with the cell electric current, which is a characteristic of the free-

molecule and transition flow regimes. For these flow regimes, the flow diffusion coefficients are weak functions of the vapor mass flow rate. For a radiation shield clearance of 48 mm, the effective geometric factor for the total pressure losses on the cathode side of the cell was $G = 143$.

The present vapor pressure loss model was also used to optimize the chevron's geometry for minimizing the vapor pressure loss through the shield. For the shield geometry that ensured minimum blockage of all direct radiation between the BASE tubes and the condenser ($\alpha = 0$), the lowest pressure loss occurred when the chevron's angle was about 60 deg, and using four or five chevrons. The vapor pressure loss was not particularly sensitive to the chevron's angle near the optimum value, allowing some tolerance for manufacturing the shield. The pressure loss through the chevron's shield increased quickly as α was increased. In the case of separated conical chevrons, the optimum geometry had three or four chevrons, with an angle of 62 deg, for which the pressure loss was about 25% higher than that in nonseparated chevrons.

Acknowledgments

This research is funded by the Space Vehicle Technologies Branch's Power and Thermal Group of the U.S. Air Force Research Laboratory, Kirtland Air Force Base, Albuquerque, New Mexico, under Contract F29601-96-K-0123, to the University of New Mexico's Institute for Space and Nuclear Power Studies.

References

[1]El-Genk, M. S., and Tournier, J.-M., "Recent Advances in Vapor-Anode, Multi-Tube, Alkali Metal Thermal-to-Electric Conversion Cells for Space Power," *Proceedings of the 5th European Space Power Conference (ESPS-98)*, SP-416, European Space Agency Publications Division, 1998 (Paper 1046).

[2]Tournier, J.-M., and El-Genk, M. S., "A Vapor Flow Model for Analysis of Liquid-Metal Heat Pipe Startup from a Frozen State," *International Journal of Heat and Mass Transfer*, Vol. 39, No. 18, 1996, pp. 3767–3780.

[3]Johnson, G. A., "Study of the Rarefied Sodium Vapor Flow in the Pluto Fast Flyby AMTEC Cell," *Proceedings of the 11th Symposium on Space Nuclear Power and Propulsion*, edited by M. S. El-Genk, AIP CP 301, Vol. 2, American Institute of Physics, New York, 1994, pp. 581–585 (CONF-940101).

[4]Ivanenok, J. F., III, Sievers, R. K., and Schultz, W. W., "Modeling of Remote Condensing AMTEC Cells," *Proceedings of the 11th Symposium on Space Nuclear Power and Propulsion*, edited by M. S. El-Genk, AIP CP 301, Vol. 3, American Institute of Physics, New York, 1994, pp. 1501–1506 (CONF-940101).

[5]Schock, A., and Or, C., "Coupled Thermal, Electrical, and Fluid Flow Analyses of AMTEC Multitube Cell with Adiabatic Cell Wall," *Proceedings of the 2nd Space Technology and Applications International Forum (STAIF-97)*, edited by M. S. El-Genk, AIP CP 387, Vol. 3, American Institute of Physics, New York, 1997, pp. 1381–1394 (CONF-970115).

[6]Schock, A., Noravian, H., Or, C., and Kumar, V., "Parametric Analyses of AMTEC Multitube Cells and Recommendation for Revised Cell Design," *Proceedings of the 2nd Space Technology and Applications International Forum (STAIF-97)*, edited by M. S. El-Genk, AIP CP 387, Vol. 3, American Institute of Physics, New York, 1997, pp. 1395–1404 (CONF-970115).

[7]Tournier, J.-M., El-Genk, M. S., Huang, L., and Schuller, M., "Performance Analysis of a Multitube Vapor-Anode AMTEC Cell," *Proceedings of the 32nd Intersociety Energy Conversion Engineering Conference*, Vol. 2, American Chemical Society, Washington, DC, 1997, pp. 1172–1179 (Paper 97378).

[8]Van Atta, C. M., *Vacuum Science and Engineering*, McGraw–Hill, New York, 1965, pp. 23–61.

[9]White, F. M., *Fluid Mechanics*, 2nd ed., McGraw–Hill, New York, 1991, Sec. 6.6, pp. 321–332.

[10]Idelchik, I. E., *Handbook of Hydraulic Resistance*, 2nd ed., English Edition edited by E. Fried, Hemisphere, Washington, DC, 1986, pp. 145–155.